Supplementary Information for the:

Investigating Evaporation in Gas Diffusion Layers for Fuel Cells with X-ray Computed Tomography

Iryna V. Zenyuk[1,*], Adrien Lamibrac[2], Jens Eller[2], Dilworth Y. Parkinson[5], Federica Marone[3], Felix N. Büchi[2], Adam Z. Weber[4]

[1]Department of Mechanical Engineering, Tufts University, Medford, MA 02155

[2]Electrochemistry Laboratory, [3]Swiss Light Source, Paul Scherrer Institut, 5232 Villigen PSI, Switzerland

[4]Energy Storage and Distributed Resources Division, [5]Advanced Light Source, Lawrence Berkeley National Laboratory, 1 Cyclotron Road, Berkleey CA 94720, USA

*Tel. number: 617-627-7956 Fax number: 617-627-3058 e-mail: Iryna.Zenyuk@tufts.edu

The Supplementary Material is composed of the following sections:

1. Effect of water surface area parsing
2. Effect of hydrophobic plug on evaporation measurements
3. Evaporation rate for S #1
4. Evaporation rate for various flow-rates for sample holder with channel
5. Evaporation rate for idealized water fronts
6. Evaporation rate theory overview

1. *Effect of Water Surface Area Parsing*

Table S1. Water surface area parsing and resulting percentage error.

Parsing	Number of triangles in isosurface	Surface Area [m^2]x10^{-6}	% Error
1	5283676	-	-
2	1287984	5.5	0
3	570864	5.38	2.18
4	314612	5.31	3.45
5	198480	5.22	5.09
6	136796	5.11	7.09

2. *Effect of Hydrophobic Plug on Evaporation Measurements*

The hydrophobic plug is modeled as a porous media with a porosity of 0.74 (manufacturer specifications) and tortuosity of 1. The thickness of the hydrophobic plug was measured from the images to be 75 µm. Diffusion resistance of gas transport through the hydrophobic plug can be thought of as a resistance in series with the resistance due to gas diffusion through the GDLs – the higher the gas transport resistance through the GDLs (higher tortuosity, lower porosity), the higher its contribution to the total resistance and the more negligible the hydrophobic plug is. Figure S1 shows the effects of the hydrophobic plug on the evaporation-rate measurements.

Only for S #1, where the water front was significantly advanced at high saturations we expect evaporation rate to be effected significantly by as much as 50%. For S #1 at saturations below 0.25 and for the other samples tested water front remained within the bottom portion of the GDL and with the large diffusion distance and lower GDL porosity the hydrophobic plug was not impacting the measurements.

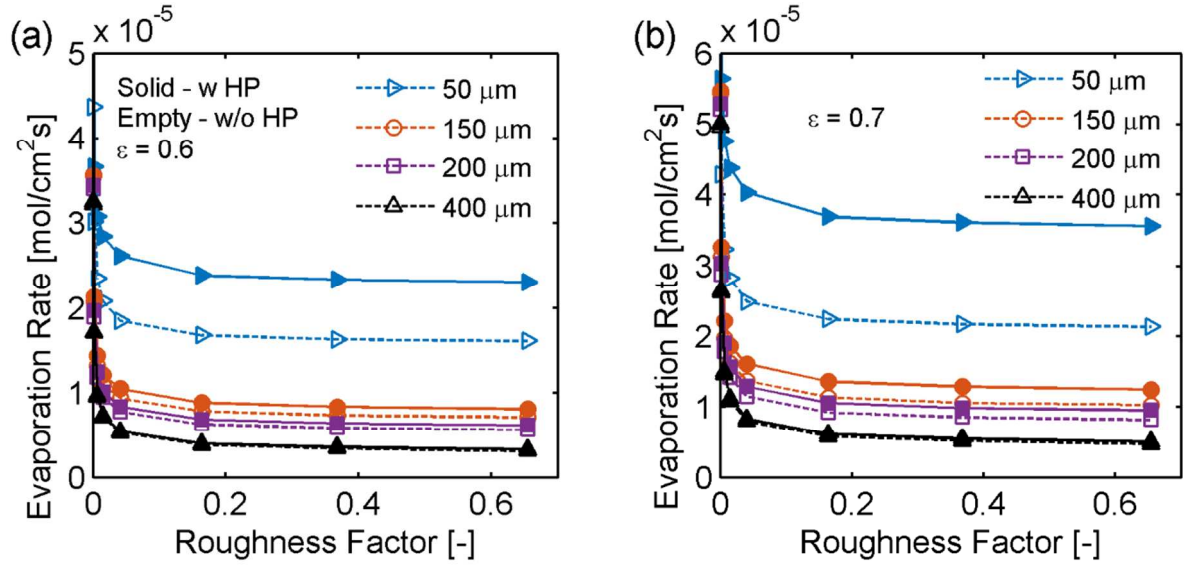

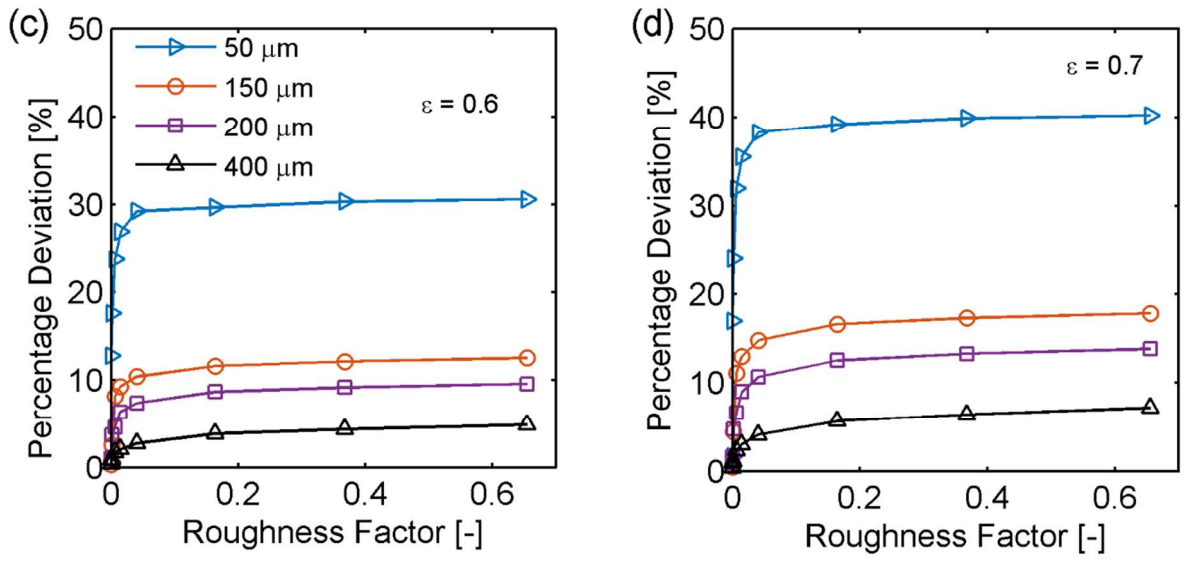

Figure S1. Evaporation rate as a function of water RF for GDLs with various thicknesses for GDLs simulated with and without hydrophobic plug (HP) on top of the GDLs for porosity a) 0.6 and b) 0.7. c) and d) Percentage deviation in evaporation rate due to HP on the top of GDL is computed for porosity of a) 0.6 and b) 0.7.

For the S #1 evaporation rate as a function of water area and saturation are shown in Figure S2. The model predicts increasing evaporation rate with liquid water saturation above 0.25 and this is due to the fact that water front has advanced to the very top of the GDL as seen in Figure S2, where volume-rendered water fronts are shown for different saturation levels. As water-front moves towards the top of the GDL the evaporation diffusion distance is decreasing and the evaporation rate increases per surface area of water because of lower diffusion distance. This was not supported by the experiments, where at 0.4 saturation the evaporation rate remained at 0.4 mol/m^{2}s – similar to that at lower saturation due to limitations of gas transport due to hydrophobic plug.

3. Evaporation Rate for S #1

Variation of evaporation rate for SGL 10 BA with increased liquid pressure is shown by Figure S2. We explore evaporation rate for a single GDL (1x), S #1 and two stacked GDLs (2x), S #2. As Figure S2a shows, with increase in water surface area (higher liquid pressure) evaporation rate decreases and then remains at nearly constant value of 0.4 mol/m^{2}s for both samples. This is indicative that evaporation rate scales with surface area of water. The model predicts the increase in evaporation rate at saturations of 0.26 or higher and this is because water front has advanced close to hydrophobic plug and diffusion distance decreased. The discrepancy between the experiment and model results is due to hydrophobic plug presence.

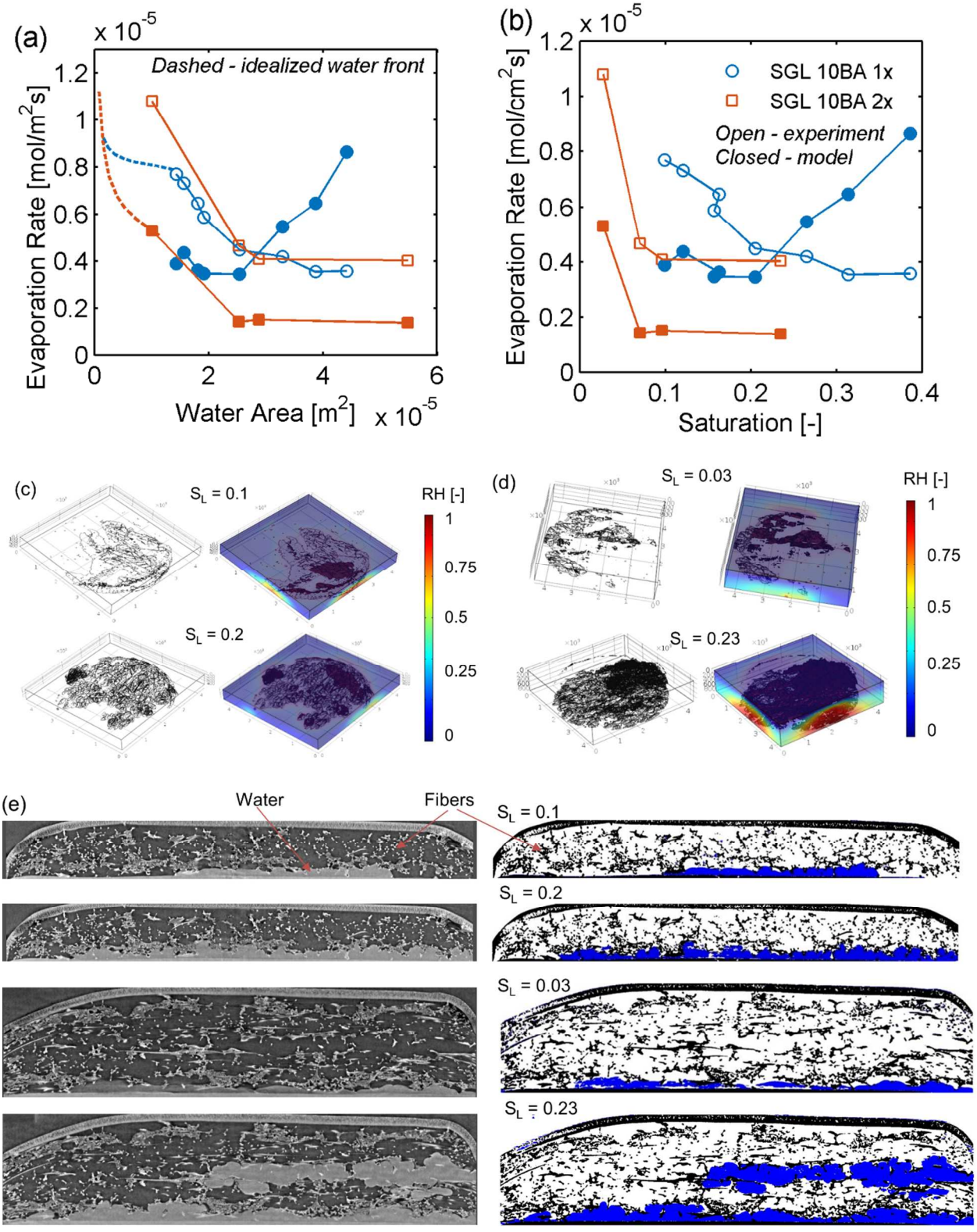

Figure S2. Evaporation rate as a function of a) water surface area and b) saturation. Volumetric mesh of water front for c) SGL 10BA 1x and d) SGL 10BA 2x for two levels of water saturation. e) Cross-section thresholded tomograph of water fronts for single and double GDL layers.

4. *Evaporation Rate for Various Flow-Rates for Sample Holder with Channel*

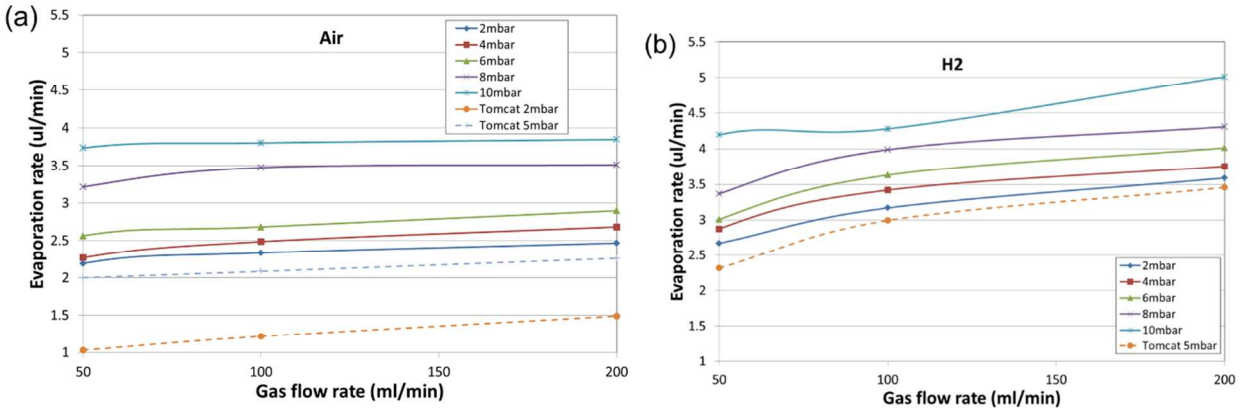

Figure S3. Evaporation rate as a function of gas flow-rate at different liquid pressures for a) air and b) hydrogen.

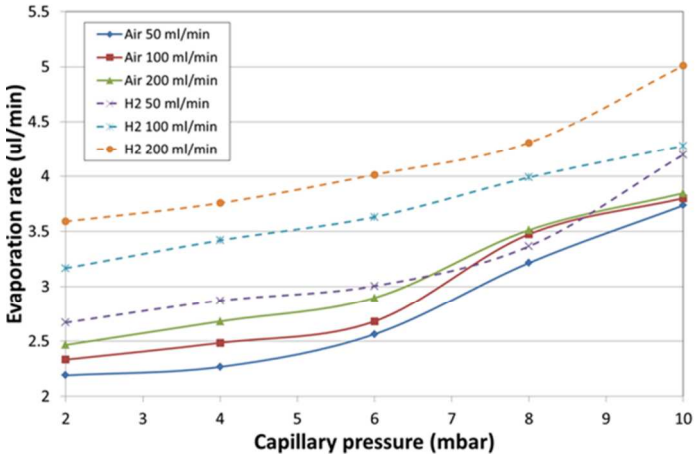

Figure S4. Evaporation rate as a function of capillary pressure for air and hydrogen at various flow-rates.

5. *Evaporation Rate for Idealized Water Fronts.*

To further understand the evaporation rate dependency on height of water front and surface area an idealized water front simulations study was conducted, where the water front was represented with cylinders of various height. The GDL domain was modeled as SGL 10 BA at 40 ^{o}C. Evaporation rate as a function of saturation is represented in Figure S5a, whereas as a function of surface area with Figure S5b. On these plots H_{front} is the normalized height of water front, which is defined as a ratio of water height, h_{water}, to GDL thickness, h_{GDL}:

$$H_{front} = \frac{h_{water}}{h_{GDL}} \quad [S1]$$

where H_{front} = 1 indicates water has reached the gas-flow channel and H_{front} = 0, it is at the interface between GDL and injection plate. Figure S5a clearly shows that evaporation rate is not as much a function of saturation as it is a function of H_{front}. For example, for H_{front} of 0.75 evaporation rate remains around 2.4×10^{-5} mol/cm^{2}s for saturation range of 0.15 – 0.5. We also observe that for H_{front} equal or larger than 0.5 evaporation rate remains approximately constant for the idealized geometries studied. For H_{front} lower than 0.5 evaporation rate shows trends similar to those observed by experiments – higher evaporation rates normalized per surface area of water at lower saturation. And this can be explained by the fact that at saturations lower than 0.08 disconnected water clusters are present and local evaporative flux is high - this flux is not offset by larger diffusion distance.

We also analyze evaporation rate as a function of water surface area as shown by Figure S5b, where increase in surface area for the same value of H_{front} leads to decrease in evaporation rate. Figure S5c shows the distribution for various cylindrical geometries of water front to obtain Figure S5a and b data. Plots on the left show water front that is only 0.12 advanced into the media, whereas on the right water front is at the height of 0.75 and depending on number and size of cylinders (the number ranged from 2 to 16) various liquid water saturation.

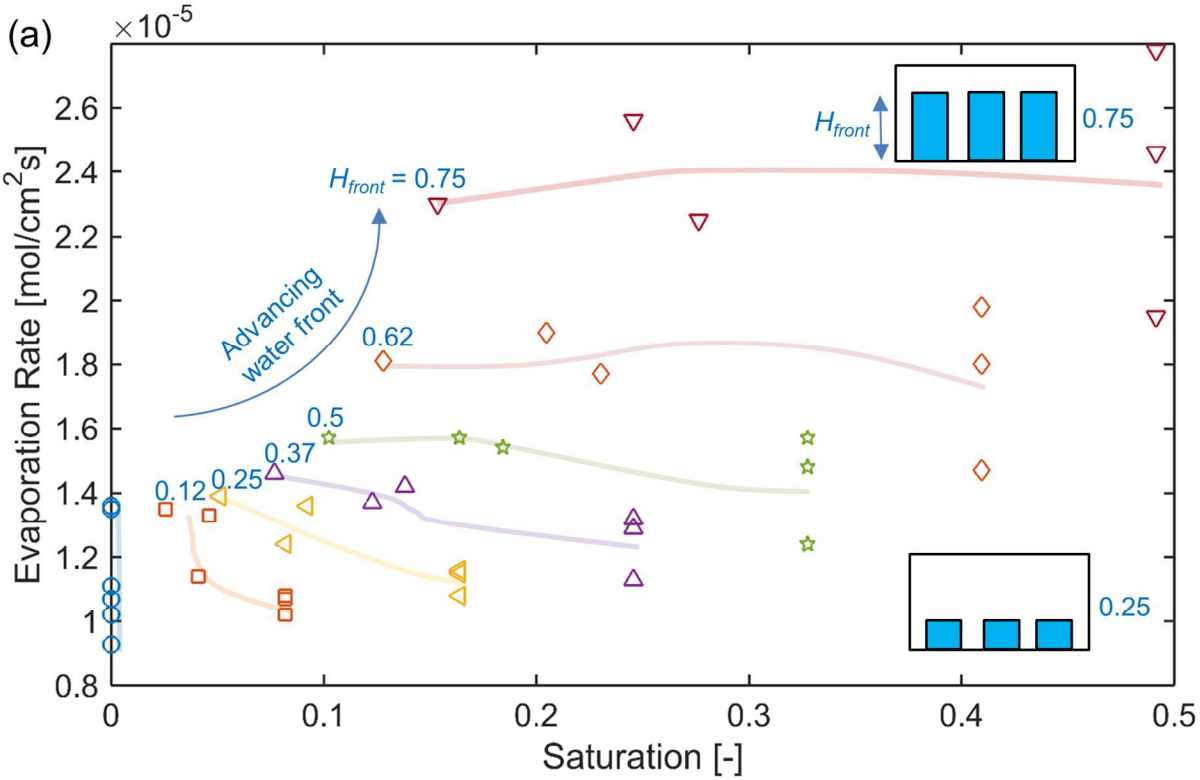

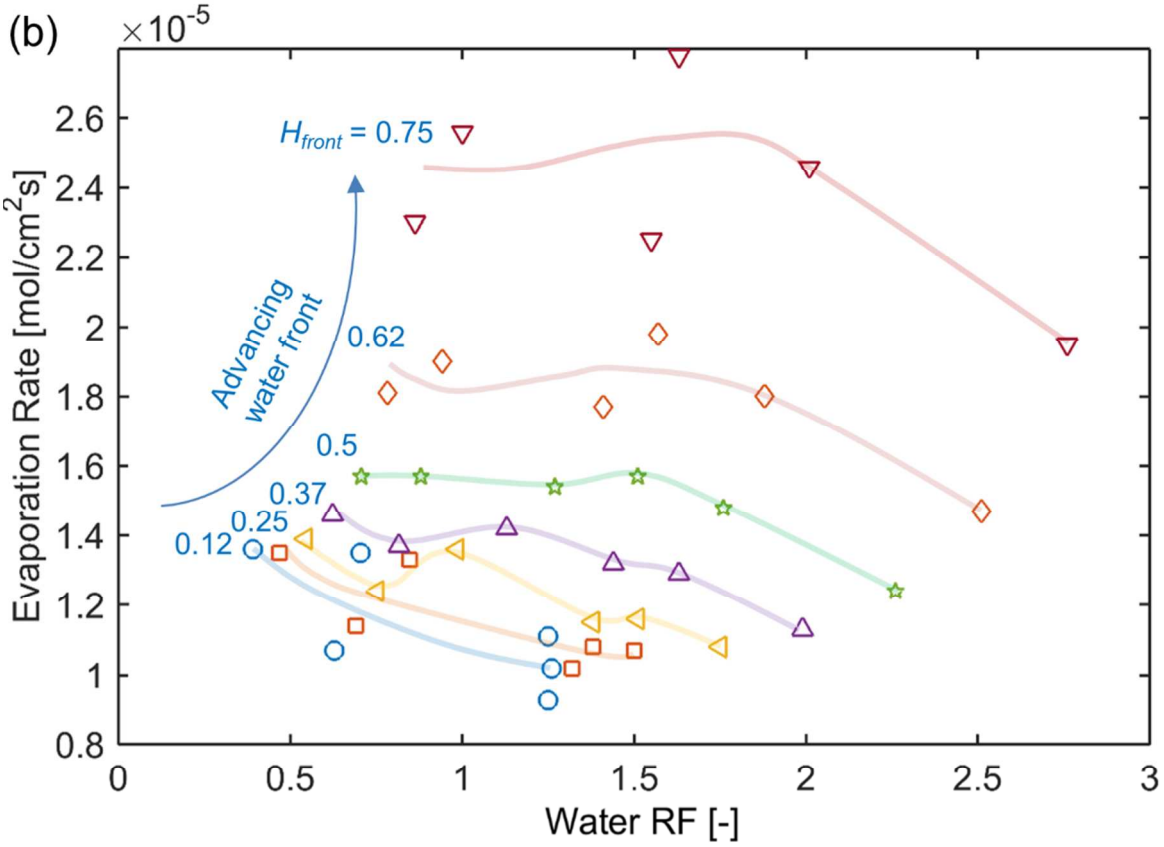
(b)
×10^-5
Evaporation Rate [mol/cm^2s]
Water RF [-]
H_front = 0.75
Advancing water front
0.62
0.5
0.37
0.25
0.12
0.8
1
1.2
1.4
1.6
1.8
2
2.2
2.4
2.6
0
0.5
1
1.5
2
2.5
3

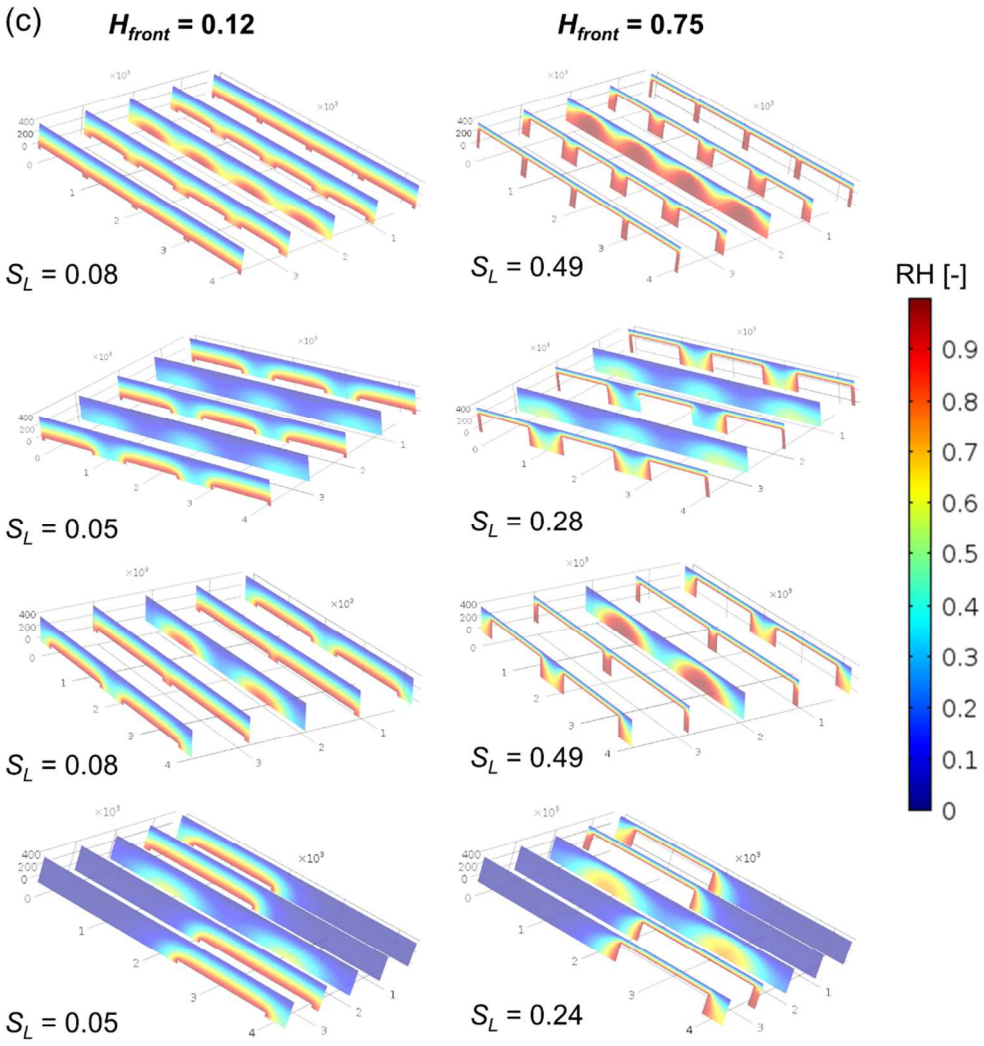

Figure S5. Evaporation rate as a function of a) saturation and b) surface area for various theoretical water-front geometries, where several of those are depicted by c).

6. Evaporation Rate Theory Overview

Under thermodynamic equilibrium at the vapor-liquid interface, temperatures ($T_l = T_v$), pressure ($P_L = P_v = P_{sat}$) and chemical potential ($\mu_L = \mu_v$) are continuous. During evaporation, non-equilibrium conditions exist at vapor-liquid interface and temperature discontinuity at liquid-vapor interface was found to be nearly 10^{o}C and chemical potential change of tens of Js [1]. The physics of interfacial kinetics are attempted to be described with classical kinetic theory o2f gases (KTG)[2-3], statistical rate theory (SRT)[4] and more recently non-equilibrium thermodynamics (NET)[5].

In the KTG a Knudsen layer exists at the vapor-liquid interface and a temperature jump occurs across this layer, therefore this temperature gradient is a driving force for the evaporating liquid. It is observed that liquid water is at lower temperature than adjacent vapor[1]. Therefore, energy ins transferred to liquid film from both bulk liquid and vapor. According to the Hertz-

Knudsen (KTG) theory, the net evaporation rate can be expressed as the difference between the evaporation and condensation fluxes:

$$J = \frac{1}{\sqrt{2\pi MR}}\left[\eta_e \frac{P_{sat}(T_L)}{\sqrt{T_L}} - \eta_c \frac{P_V}{\sqrt{T_V}}\right] \quad [S2]$$

where T_L and T_V are liquid and vapor temperatures, respectively, $P_{sat}(T_L)$ is saturated vapor pressure, P_V is vapor pressure at the vapor boundary of Knudsen layer, M is molar mass and R is ideal gas constant. The evaporation and condensation coefficients, η_e and η_c, respectively, were introduced into this expression because measured evaporation values are generally lower than those predicted by KTG theory. The evaporation coefficient was defined by Knudsen as the ratio between the number of molecules transferred to the vapor phase to those emitted from the liquid phase. Evaporation coefficient of 1 indicates that all emitted molecules from the water surfaces remained in vapor phase. For water evaporation coefficient was reported between 10^{-3} and 1 for pressure decrease from 1 to 0.01 bar[6]. When considering $\eta_e = \eta_c$ [6], and correcting bulk velocity of vapor, Schrage correction to Hetz-Knudsen can be shown as:

$$J = \frac{2\eta_e}{2-\eta_e}\sqrt{\frac{1}{2\pi R}}\left[\frac{P_{sat}(T_L)}{\sqrt{T_L}} - \frac{P_V}{\sqrt{T_V}}\right] \quad [S3]$$

SRT was developed by Ward and Fang [4] and is based on entropy difference across vapor-liquid interface. The theoretical approach is based on quantum-thermodynamics, where thermodynamics are based on the Boltzmann definition of entropy. Salient details are provided here, whereas the detailed derivation can be found elsewhere [7-8].

$$J \approx 2K_e \frac{1}{R}\Delta s_{LV} \approx 2\sqrt{\frac{1}{2\pi MRT_L}}P_{sat}(T_L)\left[\frac{1}{RT_L\rho_L}(P_V - P_{sat}(T_L)) + \frac{P_{sat}(T_L)}{P_V} - 1 + \frac{2MH\sigma}{R\rho_L T_L} - 2\left(\frac{T_V}{T_L} - 1\right)^2\right] \quad [S4]$$

Where K_e is the equilibrium molecular exchange rate between liquid and vapor, Δs_{LV} is the entropy change due to molecules exchange between liquid and vapor, 2H is mean radius of curvature. The last two terms can be neglected and the rest linearized to arrive at the following approximation:

$$J \approx 2\sqrt{\frac{1}{2\pi MRT_L}}\left(P_{sat}(T_L) - P_V\right) \quad [S5]$$

The linear form of the SRT theory is similar to KTG with $\eta_e = \eta_c = 1$. Therefore, here we will not consider SRT theory.

In the NET theory heat and mass transfer across the vapor-liquid interface is considered, and Onsager transfer coefficients are introduced. The entropy production is considered from non-equilibrium thermodynamics and full derivation can be found elsewhere [5, 8]. The final form of heat and mass transfer rates are:

$$J_q = -l_{qq}^s \frac{T_V - T_L}{T_V} - l_{qw}^s R T_L \ln \frac{P_V}{P_{sat}(T_L)} \quad [S6]$$

$$J_w = -l_{wq}^s \frac{T_V - T_L}{T_V} - l_{ww}^s R T_L \ln \frac{P_V}{P_{sat}(T_L)} \quad [S7]$$

Where l_{qq}^s, l_{ww}^s are diagonal and l_{qw}^s, l_{wq}^s are cross transfer coefficients of Onsager matrix, where the later two are equal. These relations describe evaporation transport driven by both pressure and temperature differences across the interface. It remains unknown what driving force is dominant.

References

1. Fang, G.; Ward, C. A., Temperature Measured Close to the Interface of an Evaporating Liquid. *Physical Review E* **1999**, *59*, 417-428.
2. Hertz, H., Ueber Die Verdunstung Der Flüssigkeiten, Insbesondere Des Quecksilbers, Im Luftleeren Raume. *Annalen der Physik* **1882**, *253*, 177-193.
3. Knudsen, M., Die Maximale Verdampfungsgeschwindigkeit Des Quecksilbers. *Annalen der Physik* **1915**, *352*, 697-708.
4. Ward, C. A.; Fang, G., Expression for Predicting Liquid Evaporation Flux: Statistical Rate Theory Approach. *Physical Review E* **1999**, *59*, 429-440.
5. Bedeaux, D.; Kjelstrup, S., Transfer Coefficients for Evaporation. *Physica A: Statistical Mechanics and its Applications* **1999**, *270*, 413-426.
6. Marek, R.; Straub, J., Analysis of the Evaporation Coefficient and the Condensation Coefficient of Water. *International Journal of Heat and Mass Transfer* **2001**, *44*, 39-53.
7. Rahimi, P.; Ward, C. A., Kinetics of Evaporation: Statistical Rate Theory Approach. *International Journal of Thermodynamics* **2005**, *8*, 1-14.
8. Badam, V. K.; Kumar, V.; Durst, F.; Danov, K., Experimental and Theoretical Investigations on Interfacial Temperature Jumps During Evaporation. *Experimental Thermal and Fluid Science* **2007**, *32*, 276-292.